Journal of Biomedical Optics

BiomedicalOptics.SPIEDigitalLibrary.org

Plasmonic imaging of subcellular electromechanical deformation in mammalian cells

Yunze Yang
Xianwei Liu
Shaopeng Wang
Nongjian Tao

SPIE.

Yunze Yang, Xianwei Liu, Shaopeng Wang, Nongjian Tao, "Plasmonic imaging of subcellular electromechanical deformation in mammalian cells," *J. Biomed. Opt.* **24**(6), 066007 (2019), doi: 10.1117/1.JBO.24.6.066007.

Plasmonic imaging of subcellular electromechanical deformation in mammalian cells

Yunze Yang,[a,b,†] Xianwei Liu,[c,†] Shaopeng Wang,[a] and Nongjian Tao[a,b,d,*]
[a]Arizona State University, Biodesign Institute, Center for Bioelectronics and Biosensors, Tempe, Arizona, United States
[b]Arizona State University, School of Electrical, Computer and Energy Engineering, Tempe, Arizona, United States
[c]University of Science and Technology of China, CAS Key Laboratory of Urban Pollutant Conversion, School of Chemistry and Materials Science, Hefei, China
[d]Nanjing University, State Key Laboratory of Analytical Chemistry for Life Science, School of Chemistry and Chemical Engineering, Nanjing, China

Abstract. A membrane potential change in cells is accompanied with mechanical deformation. This electromechanical response can play a significant role in regulating action potential in neurons and in controlling voltage-gated ion channels. However, measuring this subtle deformation in mammalian cells has been a difficult task. We show a plasmonic imaging method to image mechanical deformation in single cells upon a change in the membrane potential. Using this method, we have studied the electromechanical response in mammalian cells and have observed the local deformation within the cells that are associated with cell–substrate interactions. By analyzing frequency dependence of the response, we have further examined the electromechanical deformation in terms of mechanical properties of cytoplasm and cytoskeleton. We demonstrate a plasmonic imaging approach to quantify the electromechanical responses of single mammalian cells and determine local variability related to cell–substrate interactions. [DOI: 10.1117/1.JBO.24.6.066007]

Keywords: cell electromechanics; plasmonic imaging; electromechanical coupling; electromechanical deformation.

Paper 190048R received Feb. 25, 2019; accepted for publication May 30, 2019; published online Jun. 20, 2019.

1 Introduction

Electricity is a fundamental driving force in biological systems.[1] It often acts in terms of a mechanical response.[2–5] Important examples include electrically regulated beating of heart cells,[6,7] auditory sensing of hair cells,[7–9] and conformational changes in voltage-gated ion channels.[10,11] This electromechanical coupling effect is anticipated from thermodynamics, e.g., the Lippmann equation, which relates electrical potential-induced surface tension to surface charge density. However, the underlying molecular scale mechanism, especially in biological systems, is still largely unknown. An experimental challenge in studying this effect is that the electromechanical deformation at the single cell level is on the subnanometer to nanometer scale.[4,12,13] Biologically, the cell tension is subject to many factors, such as the change of cell cycles,[14–17] cell migration status,[18] cell types,[19–21] pharmaceutical environment,[22] and the number may vary for more than 10 times. Atomic force microscopy (AFM) can probe the mechanical deformation,[12,13,23–25] but it involves the contact of the AFM tip to the cells. AFM is also limited to the study of the top surface of cells and is unable to directly measure the bottom surface of cells, as well as the cell–substrate interactions. Newly developed technologies, including the piezoelectric nanoribbon transducer,[26] and optical methods, such as spectral-domain optical coherence phase microscopy (SD-OCT),[27] have been applied to mechanical deformation measurement. They either measure one location at a given time or the whole cell, which is insufficient to resolve subcellular responses. Quantitative phase microscopy provides subcellular imaging resolution, but the subtle potential-induced mechanical deformation at subcellular level has not been studied.[28]

Here we have shown a plasmonic imaging method to quantify the subnanometer cell deformation at cell–substrate interface. We studied the cell electromechanical responses and quantified the subcellular mechanical deformation at various membrane potential polarization levels and frequencies. We further modeled the cell electromechanical responses and investigated the effect of mechanical perturbations on cytoskeletons.

2 Experiments

2.1 *Cell Culture*

Wild-type HEK293T cells (ATCC, CRL-3216) were seeded on a fibronectin (Sigma, f1141)-coated gold film one day before the experiment. Cells were cultured in DMEM (Lonza) medium with 10% FBS (Life Technologies, 10437077) according to the user's manual from ATCC. After overnight incubation in 5% CO_2-humidified atmosphere at 37°C, the cells attached to the sensor surface and were ready for experiment.

2.2 *Electrophysiology*

Cultured cells were recorded at room temperature in whole-cell configuration using Axopatch 200B system (Axon Instruments). Two Ag/AgCl electrodes were used for both patch electrode and

*Address all correspondence to Nongjian Tao, E-mail: njtao@asu.edu

†These authors contributed equally to this work

bath electrode. Membrane potential was modulated sinusoidally from −60 mV to 140 mV in the voltage-clamp mode. Electrical current was simultaneously recorded. Electrical data were recorded at the sampling rate of 10,000. Glass micropipettes were pulled using a flaming puller (P-97, Sutter Instrument, California). Intracellular recording solution containing 10 mM NaCl, 135 mM K-gluconate, 10 mM HEPES, 2 mM $MgCl_2$, 2 mM Mg-ATP, and 1 mM EGTA (pH 7.4) was injected to the tip of pulled micropipettes. Micropipettes with typical resistance of 3 to 10 MΩ was used for recording. The extracellular recording solution contains 135 mM NaCl, 5 mM KCl, 1.2 mM $MgCl_2$, 5 mM HEPES, 2.5 mM $CaCl_2$, and 10 mM glucose at pH 7.4. For the step sweep experiment, membrane potential was hyperpolarized or depolarized to levels of −80, −20, 40, and 100 mV from its resting potential of −60 mV for 10 ms (see Supplementary Material—supporting note 5 and Fig. 3(c), for more details). To depolymerize the actin structure, cells were incubated at 37°C for 30 min in 10 μM cytochalasin D-containing media before measurements. Control cells were maintained in the normal culture media. Experiments with and without CD-treated cells were performed in the normal recording media.

2.3 *Plasmonic Imaging*

An inverted microscope (IX81, Olympus) with a 60× NA 1.49 oil immersion objective was implemented in the plasmonic imaging system. P-polarized light beam from a 670-nm superluminescent light-emitting diode (SLD-26-HP, Superlum) was introduced into the microscope via a total internal reflection fluorescence tube lens (TIRF module, Olympus) and a 50/50 beam splitter (Thorlabs). The reflected light from the gold surface was detected by a complementary metal-oxide semiconductor (CMOS) camera (Pike, Allied Vision) with the full resolution (640 px × 480 px) recording at 106.6 frames per second (fps). To reveal the spectral response of the cell, an ultrafast CMOS camera (Phantom V310, Vision Research) with a frame rate of 1000 fps was used. For step hyperpolarization and depolarization experiment, 10,000 fps was applied to match the electrical sampling rate. Cameras were externally triggered by the patch clamp voltage controller for synchronization. Sensor chips were made from BK-7 glass coverslips by evaporated coating of ∼1.5-nm chromium layer and a ∼47-nm gold layer on top. Chips were rinsed with deionized water and ethanol before cell plating. Cells were cultured in a removable Flexi-Perm (Sarstedt) silicone cell culture chamber placed on top of the chip surface.

2.4 *Deformation Calculation*

Raw plasmonic images were smoothed over 5 × 5 pixels (600 × 600 nm on a Pike camera) spatially to minimize pixel noise. Fast Fourier transform (FFT) was applied to the images along time. Amplitude and phase-shift images at the modulation frequency were obtained. Applied micropipette potential was used as a reference for phase-shift calculation. The Z-axis displacement was quantified by Eq. (1) from the FFT amplitude image. For potential step experiments, image sequences were aligned with polarization steps. Multiple cycles were run on each potential step repeatedly. Image sequences were averaged over multiple cycles to enhance the signal-to-noise ratio. Local deformation profile was plotted and calculated for each potential step with 5-ms moving average smoothed over time. Spectral response was fitted with linear equation in logarithm scale. All postacquisition analyses were carried out using custom-written MATLAB scripts.

3 Results and Discussion

We quantify the cell deformation using plasmonic imaging. The imaging system was built on top of an inverted optical microscope. Incident light was coupled into the microscope via a high numerical aperture objective. Reflection light from a gold-coated cover glass is imaged by a CMOS camera [Fig. 1(a)].[29–31] We manually tuned the incident angle close to the surface plasmon resonance angle to generate an evanescent field near the gold surface (Supplementary Material—supporting note 4). Since the evanescent field decays exponentially into the solution from the surface with a decay length of only about 100 nm, the plasmonic imaging is extremely sensitive to the mechanical deformation perpendicular to the surface (z-direction) (for detailed theoretical calculations, please refer to previous studies[32–34]). The deformation can be quantified according to the following equation:

$$\frac{\Delta I}{I} = 1 - \exp\left(-\frac{\Delta z}{L}\right),$$

where $\frac{\Delta I}{I}$ is the relative intensity change after cell deforms; Δz is the displacement in z-direction; and L is the decay length of the evanescent wave on the surface, which is ∼100 nm in our current imaging setting (Supplementary Material—supporting note 1).[35,36]

We cultured HEK293T cells on top of the gold sensing surface. The evanescent field interacts with the bottom part of the cell, and the deformation of the cell is recorded in the plasmonic images. To study the membrane potential-induced deformation, we controlled the potential across the cell membrane with a patch-clamp micropipette and simultaneously recorded the plasmonic images when the membrane potential was polarized. The corresponding polarization current was also recorded electrically. Since the deformation was extremely small, we applied a sinusoidal waveform to repeatedly measure this electromechanical response [Fig. 1(b)]. FFT was performed on the recorded images over time [Fig. 1(c)] and the noise at frequencies other than the one at the applied alternating potential was removed (Supplementary Material—supporting note 5). The FFT amplitude represents the magnitude of the intensity change to the applied potential. From the FFT amplitude, we further determined local cell deformation using Eq. (1), and from the FFT phase, we obtained the deformation direction with respect to the polarity of the applied potential.

Figures 2(a) and 2(b) show the bright field and plasmonic images of a cell. A glass micropipette was pressed onto the cell membrane, and the membrane patch inside the micropipette tip was ruptured after a tight glass-membrane seal was established at the contact area. In this configuration, the electrode in the micropipette is in direct contact with the intracellular fluid, allowing precise and flexible control of the potential across the cell membrane. Since micropipette is beyond the penetration depth of the surface evanescent field, it is invisible on the plasmonic images. We then applied an alternating depolarization potential from −60 to 140 mV at 37 Hz to the cell [Fig. 2(c)]. Depolarization causes a 1-nA injection of current. Correspondingly, plasmonic images also show a pronounced response at the applied frequency [Figs. 2(d) and 2(e)]. We extracted the intensity profile from the cell area, as well as from

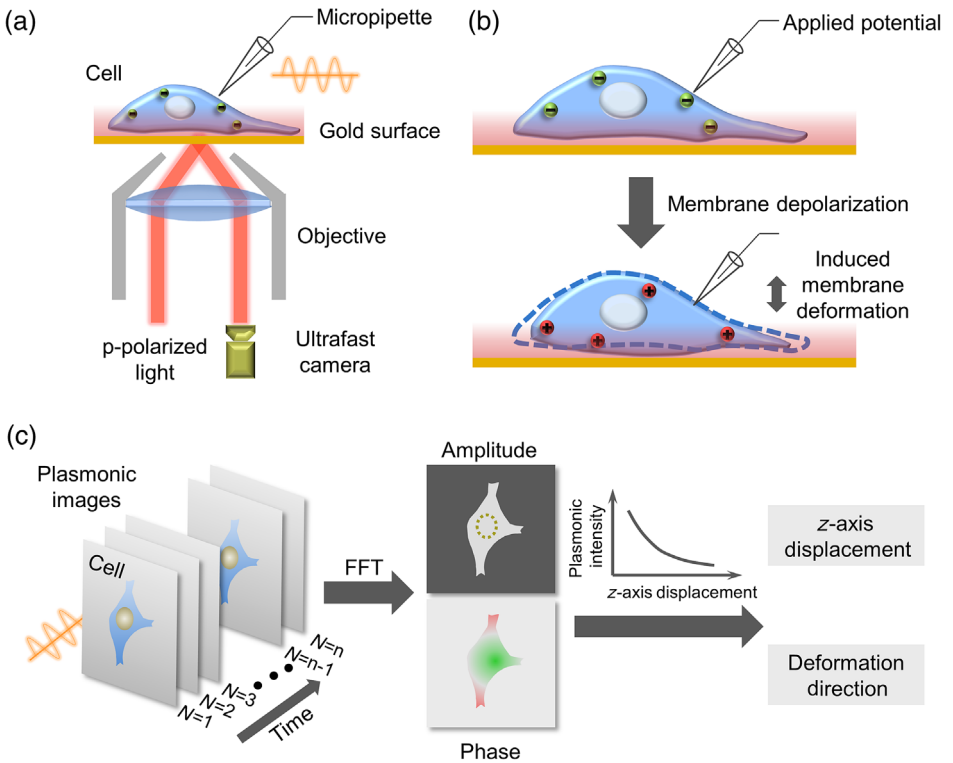

Fig. 1 Plasmonic imaging of cellular mechanical deformation. (a) Schematic diagram of experimental setup. Cells are plated on the gold-coated coverslip and are imaged with plasmonic microscopy via a fast camera. Membrane potential modulation waveform was applied to the cell with a micropipette in a whole-cell patch clamp configuration. (b) Membrane potential change induces mechanical deformation on the membrane. (c) Plasmonic images were analyzed by applying FFT along time, and the amplitude and phase-shift images at the modulation frequency were obtained, to quantify the deformation amplitude and direction.

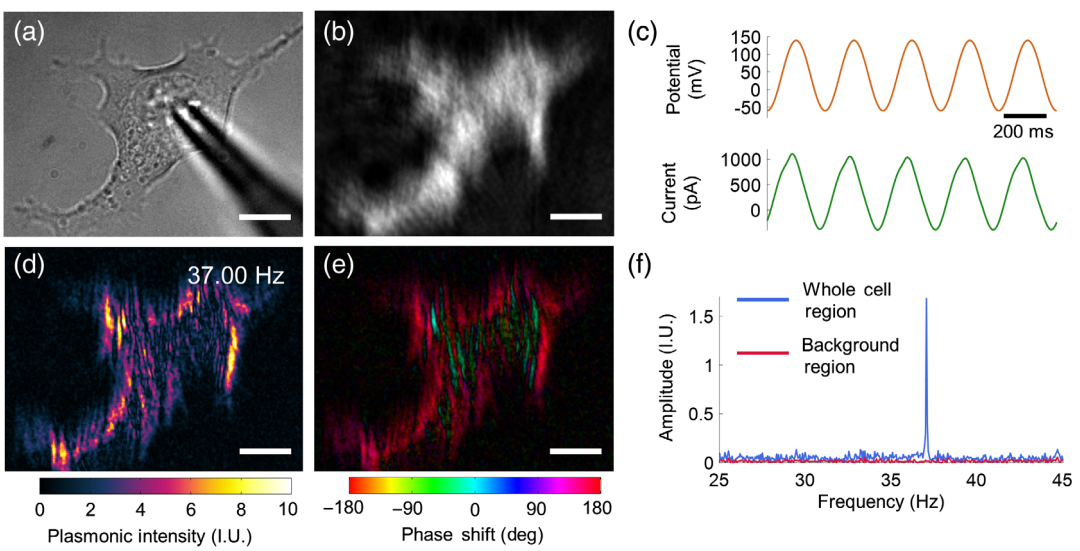

Fig. 2 Membrane potential-induced mechanical deformation in cells. (a) Transmitted and (b) plasmonic images of a cell whose membrane potential is modulated at 37 Hz using a glass micropipette. (c) Membrane potential and current associated with the potential modulation. (d) Amplitude images of the cell at the frequency of the applied potential modulation (37 Hz). (e) Phase image of the cell. (f) Spectral response of the plasmonic image intensity of the whole cell and a background region (without the cell), where the peak at the modulation frequency from the whole cell region is the mechanical deformation of the cell. Scale bar: 10 μm.

the background region without cells. A sharp peak was observed at the frequency of applied potential in the whole cell region after FFT, indicating the mechanical deformation generated from the cell by the applied potential [Fig. 2(f)]. In contrast, no obvious response was detected in the background region. From the FFT amplitude image, we observed a much bigger response at the cell edge than that from the center, suggesting a heterogeneous electromechanical deformation at different subcellular regions [Fig. 2(d)].

To quantify the time delay of the electromechanical deformation, we analyzed the phase shift of the recorded images with respect to the applied potential. Only in-phase (0 deg) and antiphase (180 deg) responses were observed in the FFT phase image at 37 Hz [Fig. 2(e)]. The cell center mainly displayed an in-phase (0 deg) response (colored as cyan), whereas the edge area was antiphase (180 deg, red). This result shows that the cell bottom deforms along with the applied potential, but cell center and edge deform in opposite directions. When the cell is depolarized, the center portion of the cell moves closer to the gold surface (intensity increase) while the edge moves away from the surface (intensity decrease) [Fig. 1(b)]. This bidirectional response rules out the possibilities that the observed plasmonic signal was from other mechanisms (Supplementary Material—supporting note 2).

To further study the relationship between mechanical deformation and membrane potential changes, we measured the mechanical responses at different potential polarization levels. The cells were electrically hyperpolarized or depolarized in potential steps from −80 to 100 mV at an interval of 60 mV per step [Fig. 3(c)]. Plasmonic images were simultaneously captured at the same sampling rate as 10,000 fps (see Supplementary Material—experiments and supporting note 5, for more details) [Fig. 3(a)]. This sequence was repeated and the plasmonic images were averaged over the repeated measurement for denoising (see methods). Figure 3(b) shows a differential image of cellular response of potential depolarization from −60 to 100 mV after averaging over 94 cycles of repeated measurements. The cell center showed an increased plasmonic intensity, whereas the cell edge showed an opposite response, which is consistent with the result presented in the previous section. The similar intensity outside the cell contour region was due to the noise from the background. To accurately quantify the dynamic response of the cell deformation, we plotted the deformation responses over the cell center and over the cell edge, respectively [Fig. 3(d)]. Both regions deformed slowly after a sudden potential polarization. However, the exact response speed is biased due to the moving average used in the denoising scheme. At the steady state, deformation magnitude showed a linear dependency on the membrane polarization for both regions [Fig. 3(e)], with an average displacement of about 0.02 nm per 100 mV at the cell edge and 0.005 nm per 100 mV at the cell center, respectively. These numbers are about one order of magnitude smaller than that of the mechanical motions tracked at the cell edge using digital microscopy.[4] This is probably due to the impeded motions at the cell–substrate interface of the adherent cells. The thermal energy-induced fluctuation is typically at the same level. However, these fluctuations were random, spanning across the whole spectrum. In our current detection scheme, we externally drive the motion. Different subcellular regions deform in a synchronous manner. Thus, the thermal fluctuation is suppressed by either averaging (as in Fig. 3) or limiting the detection bandwidth (as in Fig. 2).

Thermodynamics predicts that potential changes across the cell membrane will lead to a mechanical deformation.[12] The relationship between surface tension and potentials for a single interface is described as Lippmann equation:

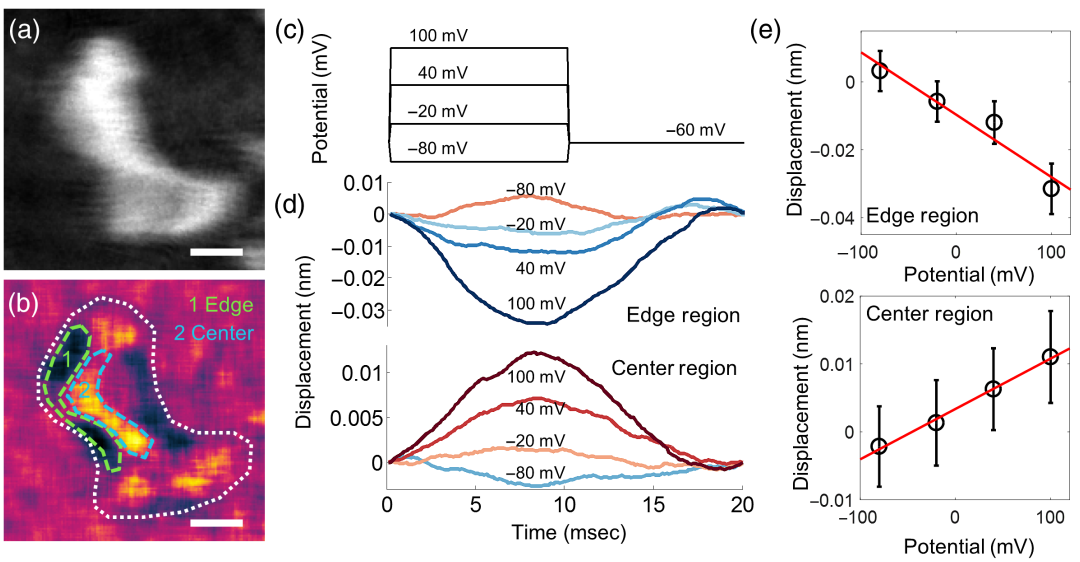

Fig. 3 Cell deformation and its dependence on the membrane potential. (a) Raw plasmonic and (b) differential plasmonic images of a depolarized cell from −600 to 100 mV, where the white line marks the edge of the cell, the green and blue dashed lines indicate a cell edge and center regions selected for quantification, respectively. (c) Stepwise change of the membrane potential polarization. (d) Time profiles of the mechanical deformation in the cell edge (top) and center (bottom) regions in response to the stepwise membrane potential polarization. (e) Relationship of the mechanical deformation in the cell edge and center regions at the steady state of each potential steps, where the error bars indicate the temporal standard deviation of the deformation for each potential step (averaged over 94 cycles). Scale bar: 10 μm.

$$\frac{\partial \gamma}{\partial V} = -q,$$

where γ is the surface tension, V is the membrane electrical potential, and q is the excess mobile charge in the double layer of the membrane surface. However, thermodynamics does not provide how much a cell will deform with a given change of membrane potential. The actual magnitude and phase of the deformation induced by the membrane surface tension is determined by the mechanical properties of the cells.

To explain the observed electromechanical response, as well as to accurately evaluate the response speed, we performed a spectral analysis on the deformation of single cells. We measured the cellular mechanical response over a wide frequency range from 7 to 312.5 Hz with a constant potential change (200 mV of depolarization from −60 mV resting potential) for each frequency. Figures 4(a)–4(e) show the responses at different modulation frequencies after FFT from the recorded plasmonic images. The amplitude is shown as the brightness and the phase-shift is encoded in color. We observed a near-in-phase and antiphase mechanical responses with respect to the applied potential modulation (0 deg and 180 deg only) over the frequencies. No other intermediate phases were detected.

The mechanical property of a cell can be modeled as

$$G = G' + iG'',$$

where G is the modulus that describes the mechanical properties of the cells.[37] It is a combination of an elastic component, described by storage modulus (G'), and a viscous component, or loss modulus (G'') [Fig. 4(f)]. The $G(f)$ is examined by calculating the ratio between applied oscillatory force $F(f)$ at frequency f and corresponding displacement $x(f)$, that is, $F(f)/x(f)$, in the frequency domain. Therefore, according to the FFT phase of the observed mechanical response [Figs. 4(a)–4(e)], the cell is mainly an elastic body, rather than a viscous one within the frequency range.

Electromechanical properties of the cell can be extracted by analyzing the relation between the displacement and the applied potential. We calculated the averaged deformation magnitude from both the cell center and the edge at different frequencies. Figures 4(g) and 4(h) show the spectral response of deformations with 200 mV depolarization at both regions. Fitted with a linear equation in log-log scale, the deformation magnitude followed a negative power-law form, $|x(f)| \sim f^{-\beta}$, with exponent β equal to 0.15 and 0.3 in edge and center regions, respectively. The storage modulus, the inverse of displacement with

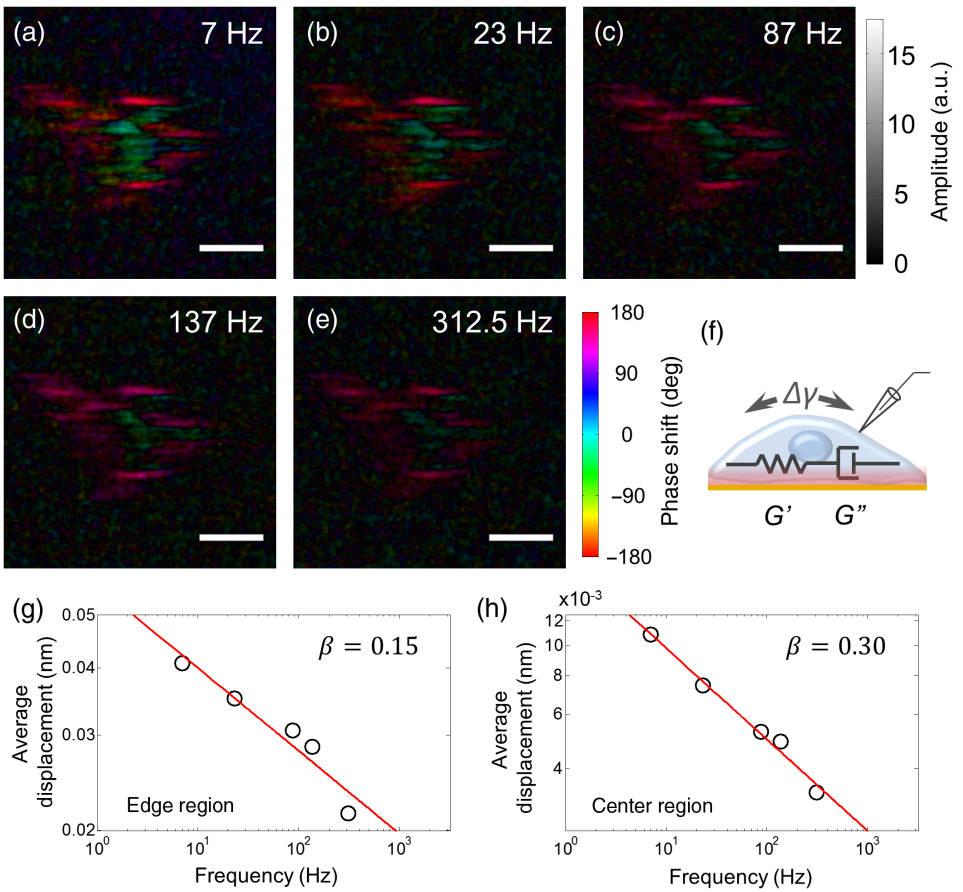

Fig. 4 Cell deformation and its dependence on the membrane potential modulation frequency. (a)–(e) FFT image of cellular mechanical deformation in response to membrane potential modulation frequencies, where the brightness and color indicate the amplitude and phase of the FFT images. (f) Mechanical model of cell deformation. (g), (h) Mechanical deformation in the cell edge and center regions versus modulation frequency, where the data are plotted in log-log scale and fitted with a linear equation. Scale bar: 20 μm.

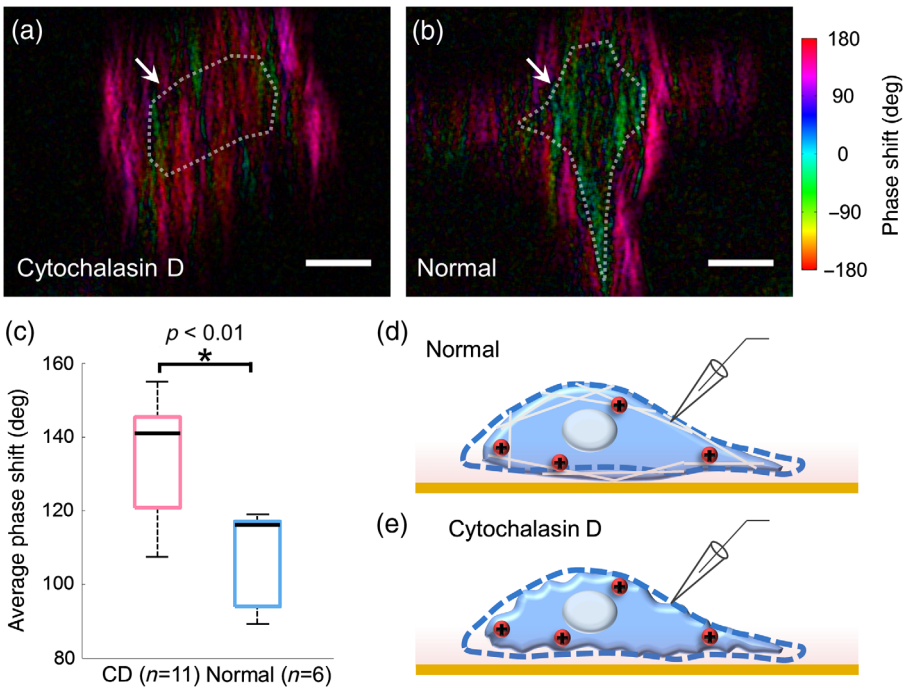

Fig. 5 Modification of the mechanical properties of the cell with cytochalasin D. (a), (b) Potential-induced cell deformation of (a) cytochalasin D-treated cells and (b) normal cells, where the white lines indicate the phase boundary. (c) Averaged phase shift of the whole cell; $p < 0.01$, t-test. (d), (e) Model illustration of the potential-induced cell mechanical deformation of the cytochalasin D-treated cells and normal cells. Scale bar: 10 μm.

the same modulation potential, is given as $|G'(f)| \sim f^{\beta}$. This result is in good agreement with previous rheological measurements using intracellular microbead- or cytoskeleton-attached magnetic nanoparticle conducted on cells.[38,39]

We anticipate that mechanical perturbation to the cellular structure will remarkably affect the electromechanical response and can be observed with plasmonic imaging (see Supplementary Material—supporting note 3, for full electromechanical model). To confirm this, we treated the cells with an actin polymerization inhibitor, cytochalasin D, and examined the corresponding electromechanical responses.[40] Actin fibers are the main component of the cytoskeleton and determine the cell mechanics.[20,41–43] After depolymerizing the actin frame structure, cell centers show an expanded anti-phase area (red) compared with those in the normal condition [Figs. 5(a) and 5(b), white dash lines]. The boundaries between the in-phase and the antiphase regions disappeared, and the in-phase regions appeared to be more random at different subcellular locations. To quantitatively examine the subcellular phase change, we quantified the average phase-shift over the whole cell area. A significant phase shift toward antiphase (180 deg) after cytochalasin D treatment was observed [Fig. 5(c), $p < 0.01$, t-test]. This result suggests that a larger portion of the cell bottom membrane moved inward synchronously after depolarization [Figs. 5(d) and 5(e)].

4 Conclusion

We have demonstrated a plasmonic method for detecting subnanometer deformation from cell electromechanical coupling. This capability allows us to visualize membrane-potential-induced cell mechanical deformation. At frequencies below hundreds of hertz, the deformation is mainly elastic. Deconstructing the actin structure revealed an important role of cytoskeleton in the observed potential-induced cell mechanical deformation. Our work shows that membrane potential-induced cell mechanical deformation can be imaged with the plasmonic method with subcellular spatial resolution and subnanometer resolution. We anticipate that the method can contribute to mechanobiological studies and shed light on the understanding of important biological functions, including mechanosensitive ion channels and protein configuration changes in voltage-gated ion channels.

Disclosures

The authors have no relevant financial interests in this article and no potential conflicts of interest to disclose.

Acknowledgments

The authors would like to thank Dr. Ming Gao and Dr. Jie Wu from Barrow Neurological Institute for their technical support on electrophysiological recordings. Research reported in this publication was supported by the National Institute of General Medical Sciences of the National Institutes of Health under Award No. R01GM107165. The content is solely the responsibility of the authors and does not necessarily represent the official views of the National Institutes of Health.

References

1. A. L. Hodgkin and A. F. Huxley, "A quantitative description of membrane current and its application to conduction and excitation in nerve," *J. Physiol.* **117**(4), 500–544 (1952).
2. I. Tasaki and K. Iwasa, "Rapid pressure changes and surface displacements in the squid giant axon associated with production of action potentials," *Jpn. J. Physiol.* **32**(1), 69–81 (1982).
3. J. K. Mueller and W. J. Tyler, "A quantitative overview of biophysical forces impinging on neural function," *Phys. Biol.* **11**(5), 051001 (2014).

4. Y. Yang et al., "Imaging action potential in single mammalian neurons by tracking the accompanying sub-nanometer mechanical motion," *ACS Nano* **12**, 4186–4193 (2018).
5. L. Cohen, "Changes in neuron structure during action potential propagation and synaptic transmission," *Physiol. Rev.* **53**(2), 373–418 (1973).
6. E. R. Pfeiffer et al., "Biomechanics of cardiac electromechanical coupling and mechanoelectric feedback," *J. Biomech. Eng.* **136**(2), 021007 (2014).
7. I. Kehat et al., "Electromechanical integration of cardiomyocytes derived from human embryonic stem cells," *Nat. Biotechnol.* **22**(10), 1282–1289 (2004).
8. R. M. Raphael, A. S. Popel, and W. E. Brownell, "A membrane bending model of outer hair cell electromotility," *Biophys. J.* **78**(6), 2844–2862 (2000).
9. J. Zheng et al., "Prestin is the motor protein of cochlear outer hair cells," *Nature* **405**(6783), 149–155 (2000).
10. F. Bezanilla, "Voltage sensor movements," *J. Gen. Physiol.* **120**(4), 465–473 (2002).
11. F. Bezanilla, "How membrane proteins sense voltage," *Nat. Rev. Mol. Cell Biol.* **9**(4), 323–332 (2008).
12. P.-C. Zhang, A. M. Keleshian, and F. Sachs, "Voltage-induced membrane movement," *Nature* **413**(6854), 428–432 (2001).
13. A. Beyder and F. Sachs, "Electromechanical coupling in the membranes of Shaker-transfected HEK cells," *Proc. Natl. Acad. Sci. U.S.A.* **106**(16), 6626–6631 (2009).
14. E. Fischer-Friedrich et al., "Quantification of surface tension and internal pressure generated by single mitotic cells," *Sci. Rep.* **4**, 6213 (2014).
15. C. J. Cattin et al., "Mechanical control of mitotic progression in single animal cells," *Proc. Natl. Acad. Sci. U.S.A.* **112**(36), 11258–11263 (2015).
16. M. Krieg et al., "Tensile forces govern germ-layer organization in zebrafish," *Nat. Cell Biol.* **10**(4), 429–436 (2008).
17. P. Chugh et al., "Actin cortex architecture regulates cell surface tension," *Nat. Cell Biol.* **19**(6), 689–697 (2017).
18. S. van Helvert, C. Storm, and P. Friedl, "Mechanoreciprocity in cell migration," *Nat. Cell Biol.* **20**(1), 8–20 (2018).
19. C. Monzel et al., "Measuring fast stochastic displacements of bio-membranes with dynamic optical displacement spectroscopy," *Nat. Commun.* **6**, 8162 (2015).
20. H. Yu et al., "Tracking fast cellular membrane dynamics with sub-nm accuracy in the normal direction," *Nanoscale* **10**(11), 5133–5139 (2018).
21. M. J. Rosenbluth, W. A. Lam, and D. A. Fletcher, "Force microscopy of nonadherent cells: a comparison of leukemia cell deformability," *Biophys. J.* **90**(8), 2994–3003 (2006).
22. A. X. Cartagena-Rivera et al., "Actomyosin cortical mechanical properties in nonadherent cells determined by atomic force microscopy," *Biophys. J.* **110**(11), 2528–2539 (2016).
23. N. Tao, S. Lindsay, and S. Lees, "Measuring the microelastic properties of biological material," *Biophys. J.* **63**(4), 1165–1169 (1992).
24. J. Mosbacher et al., "Voltage-dependent membrane displacements measured by atomic force microscopy," *J. Gen. Physiol.* **111**(1), 65–74 (1998).
25. G. Kim et al., "A mechanical spike accompanies the action potential in mammalian nerve terminals," *Biophys. J.* **92**(9), 3122–3129 (2007).
26. T. D. Nguyen et al., "Piezoelectric nanoribbons for monitoring cellular deformations," *Nat. Nanotechnol.* **7**(9), 587–593 (2012).
27. T. Akkin, C. Joo, and J. F. de Boer, "Depth-resolved measurement of transient structural changes during action potential propagation," *Biophys. J.* **93**(4), 1347–1353 (2007).
28. S. Oh et al., "Label-free imaging of membrane potential using membrane electromotility," *Biophys. J.* **103**(1), 11–18 (2012).
29. B. Huang, F. Yu, and R. N. Zare, "Surface plasmon resonance imaging using a high numerical aperture microscope objective," *Anal. Chem.* **79**(7), 2979–2983 (2007).
30. S. Wang et al., "Label-free imaging, detection, and mass measurement of single viruses by surface plasmon resonance," *Proc. Natl. Acad. Sci. U.S.A.* **107**(37), 16028–16032 (2010).
31. X. W. Liu et al., "Plasmonic—based electrochemical impedance imaging of electrical activities in single cells," *Angew. Chem. Int. Ed.* **56**(30), 8855–8859 (2017).
32. H. Raether, "Surface plasmons on smooth surfaces," in *Surface Plasmons on Smooth and Rough Surfaces and on Gratings*, H. Raether, Ed., pp. 4–39, Springer, Berlin (1988).
33. J. Homola, "Electromagnetic theory of surface plasmons," in *Surface Plasmon Resonance Based Sensors*, J. Homola, Ed., pp. 3–44, Springer, Berlin (2006).
34. S. Wang, S. Boussaad, and N. J. Tao, "Spectroscopy: applications in protein adsorption and electrochemistry," in *Biomolecular Films: Design, Function, and Applications*, J. F. Rusling, Ed., Vol. **111**, p. 213, Marcel Dekker, Inc., New York (2003).
35. Y. Yang et al., "Label-free tracking of single organelle transportation in cells with nanometer precision using a plasmonic imaging technique," *Small* **11**(24), 2878–2884 (2015).
36. X. Shan et al., "Detection of charges and molecules with self-assembled nano-oscillators," *Nano Lett.* **14**(7), 4151–4157 (2014).
37. X. Trepat, G. Lenormand, and J. J. Fredberg, "Universality in cell mechanics," *Soft Matter* **4**(9), 1750–1759 (2008).
38. B. Fabry et al., "Scaling the microrheology of living cells," *Phys. Rev. Lett.* **87**(14), 148102 (2001).
39. M. Guo et al., "Probing the stochastic, motor-driven properties of the cytoplasm using force spectrum microscopy," *Cell* **158**(4), 822–832 (2014).
40. J. F. Casella, M. D. Flanagan, and S. Lin, "Cytochalasin D inhibits actin polymerization and induces depolymerization of actin filaments formed during platelet shape change," *Nature* **293**(5830), 302–305 (1981).
41. S. M. A. Haghparast, T. Kihara, and J. Miyake, "Distinct mechanical behavior of HEK293 cells in adherent and suspended states," *PeerJ* **3**, e1131 (2015).
42. D. A. Fletcher and R. D. Mullins, "Cell mechanics and the cytoskeleton," *Nature* **463**(7280), 485–492 (2010).
43. S. Suresh, "Biomechanics and biophysics of cancer cells," *Acta Mater.* **55**(12), 3989–4014 (2007).

Yunze Yang received his BS and MS degrees in Life Science at Shanghai Jiao Tong University and completed his PhD at Arizona State University in electrical engineering in 2016. Currently, he is a postdoctoral researcher with Professor Nongjian Tao at Arizona State University. His research focuses on development of novel imaging technologies and their applications in biomedicine.

Xianwei Liu received his PhD from University of Science and Technology of China (USTC) in 2011, where he studied extracellular electron transfer. After working at the University of Illinois at Urbana-Champaign for one year, he joined the group of Professor Nongjian Tao at Arizona State University, USA, as a postdoctoral research associate. In 2016, he was appointed as a professor in the Applied Chemistry Department at USTC. His group specializes in optical imaging of interfacial chemistry processes.

Shaopeng Wang received his BS degree in biology in 1990 and MS degree in biophysics from Tsinghua University in 1993. He received his PhD in physical chemistry from University of Miami with Professor Roger M. Leblanc in 1999. After completing his two-year postdoctoral studies at the Physics Department of Florida International University with Professor Nongjian Tao, he worked as an industrial senior research scientist at ICx Nomadics Inc. In 2008, he was appointed as an associate research professor at the Biodesign Center for Bioelectronics and Biosensors at Arizona State University and was promoted to full research professor in 2015. His research focuses on the development of biosensors and bioinstrumentations for biomedical applications.

Nongjian Tao joined Arizona State University as a professor of electrical engineering and an affiliated professor of chemistry and biochemistry in August 2001. Since 2008, he has been serving as the director of the Biodesign Center for Bioelectronics and Biosensors, leading a transdisciplinary effort to develop sensors and biomedical applications at ASU. He is a fellow of the American Association for the Advancement of Science, the American Institute for Medical and Biological Engineering, and the American Physical Society. He is an associate editor for *ACS Sensors*. He has ~300 publications, 23 US patents (11 licensed or commercialized), and has given over 275 invited and keynote talks worldwide.